THE JOURNAL OF PHYSICAL CHEMISTRY C

Article

pubs.acs.org/JPCC

Nanocolumnar Germanium Thin Films as a High-Rate Sodium-Ion Battery Anode Material

Paul R. Abel,[†] Yong-Mao Lin,[†] Tania de Souza,[†] Chia-Yun Chou,[‡] Asha Gupta,[‡] John B. Goodenough,[‡] Gyeong S. Hwang,[†] Adam Heller,[†,§] and C. Buddie Mullins*[,†,‡,§,⊥]

[†]McKetta Department of Chemical Engineering, [⊥]Department of Chemistry and Biochemistry, [§]Center for Electrochemistry, and [‡]Texas Materials Institute and Center for Nano- and Molecular Science, University of Texas at Austin, 1 University Station, C0400 Austin, Texas 78712-0231, United States

Supporting Information

ABSTRACT: Both nanocolumnar and dense germanium thin films, synthesized by evaporative deposition, were tested as a potential anode material for sodium-ion batteries. The reversible capacity of the nanocolumnar films was found to be 430 mAh/g, which is higher than the theoretical capacity of 369 mAh/g. The nanocolumnar films retained 88% of their initial capacity after 100 cycles at C/5, whereas the dense films began to deteriorate after ∼15 cycles. Additionally, the nanocolumnar films were stable at charge/discharge rates up to 27C (10 A/g). The diffusion coefficient for sodium in germanium was estimated, from impedance analysis of the dense films, to be $\sim 10^{-13}$ cm^2 s^{-1}. Modeling of diffusion in the sodium- germanium system predicts that sodium diffusion in the near-surface layers of the material is significantly faster than in the bulk. These results show that small feature sizes are critical for rapid, reversible electrochemical sodiation of germanium.

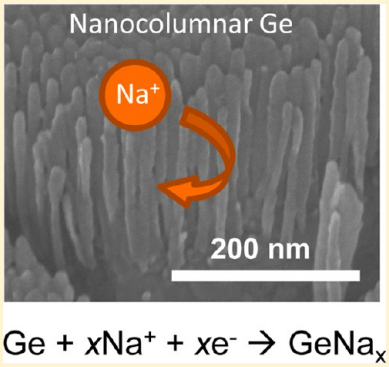

1. INTRODUCTION

Existing commercially available sodium battery chemistries such as sodium−sulfur and sodium−nickel chloride use molten electrodes, a ceramic separator, and must operate above 300 °C.[1,2] This requirement presents challenges for implementation at small scales and for on-demand applications. The development of room temperature sodium battery chemistries would therefore provide significant advantages and have the possibility to compete with currently available lithium-ion chemistries for stationary storage of electrical energy.[3]

The ongoing search for sodium insertion compounds suitable for room temperature sodium-ion batteries is impeded by the large size of the sodium ion; it is difficult to find materials that can reversibly store sodium ions with reasonable rates of charge and discharge. Layered metal oxides and phosphates similar to those used in Li-ion batteries have been shown to reversibly store the larger sodium ion.[4−8] Additionally, NASICON structured material[9−11] and cubic Prussian blue analogues[12−14] show promise as potential cathode materials. However, anode materials for room temperature sodium-ion batteries are more elusive. Unlike lithium, sodium ions do not intercalate reversibly into graphite; therefore, alternative materials are sought. Nongraphitic carbons have been investigated, but they have been found to have high first-cycle irreversible capacities and low reversible capacities.[15−17] In analogy with their use in lithium-ion batteries, alloys have been investigated to develop high-capacity sodium-ion battery anodes. Sodium is known to alloy with tin[18−20] and antimony.[21,22] Additionally, the ternary sodium−tin-antimony alloy has been considered as an anode material.[23] Chevrier and Ceder, in a very interesting study, calculated that sodium should alloy with germanium up to NaGe, giving a theoretical capacity of 369 mAh/g.[24]

Germanium has been extensively studied as an anode material for lithium-ion batteries as it has a high lithium storage capacity and high lithium diffusivity.[25−29] Sodium diffusion in crystalline germanium was studied at high temperature by Stojić et al. and found to be several orders of magnitude slower than that of lithium in germanium.[30,31] Both species are interstitial diffusers; however, the larger radius of sodium in comparison to lithium results in a much higher activation energy for hopping between interstitial sites in the lattice (0.51 eV for lithium vs 1.5 eV for sodium). For sodium-ion batteries, solid state diffusion is a significant fraction of the total cell resistance. It is well established in the literature that surface diffusion and grain boundary diffusion are both much faster than bulk diffusion in solids. It is, therefore, desirable to utilize nanostructured germanium to overcome the low bulk diffusion coefficient of sodium in germanium in order to minimize the total cell resistance.

In this paper, we investigate the electrochemical properties of dense and nanocolumnar germanium thin films synthesized by glancing angle deposition (GLAD) as candidate anode materials for sodium-ion batteries. GLAD is a physical vapor deposition technique where adatoms impinge on a surface at an oblique angle. In the early stages of deposition, stochastic variation in deposition rate roughens the surface. If surface

Received: July 23, 2013
Revised: August 20, 2013
Published: August 21, 2013

diffusion is limited, the roughness is amplified by self-shadowing (see Abelmann and Lodder for additional details on this process)[32] and nanocolumnar films can be grown.[33] In GLAD, the morphology of the film is strongly dependent on deposition angle, with films deposited at angles close to the surface normal resulting in dense films and oblique angles resulting in highly porous,[34,35] nanocolumnar films.[36] More details on this technique can be found elsewhere.[25,37−40] A previous study on how the deposition angle of TiO_2 GLAD electrodes for lithium-ion batteries affected electrochemical performance found diminishing returns in performance for angles greater than 70°.[38] For this reason, this study is limited to comparing the performance of dense films and optimally nanostructured films deposited at 70°.

2. EXPERIMENTAL SECTION

2.1. Material Synthesis. Germanium (Kurt J. Lesker, 99.999%) was vacuum deposited (by electron beam heating) onto a 15.6 mm diameter stainless steel substrate (Pred Materials) at an incident angle of either 0° (dense films) or 70° (nanocolumnar films) from the surface normal. The stainless steel substrates were cleaned by sonication in ethanol prior to deposition. The deposition rate was calibrated with a quartz crystal microbalance, and the mass density of all films was 50 $\mu g/cm^2$. The accuracy of the microbalance was checked by cross sectional SEM imaging of the films (see Figure S1).

2.2. Material Characterization. Imaging of germanium thin films was performed using a Hitachi S5500 microscope in SEM mode. TEM was performed using a JEOL 2010F transmission electron microscope. XPS was performed using a Kratos Axis Ultra X-ray photoelectron spectrometer utilizing a monochromatic Al Kα X-ray source (hν = 1486.5 eV). A charge neutralizer was employed during analysis. Sample stoichiometry was determined using Casa XPS analysis software. Sensitivity factors for each element of interest were either provided by Kratos or experimentally determined.

2.3. Electrochemical Testing. As-deposited electrodes were held in a low humidity environment for 72 h to allow for native oxide formation prior to assembly into 2032 coin cells in an argon-filled glovebox (MBraud Unilab) with oxygen and water levels held below 2 ppm. Sodium metal (Alfa Aesar, 99%) was used as the counter/pseudoreference electrode and 1 M $NaPF_6$ (Sigma Aldrich, battery grade) in a 1:1 mixture of fluorinated ethylene carbonate (Solvay Chemicals) and diethyl carbonate (sigma Aldrich, battery grade) as the electrolyte. Coin cells were galvanically cycled in an Arbin BT2043 multichannel battery tester. The cells were cycled between 5 mV and 1.5 V versus Na/Na^+. Impedance spectroscopy was performed with a CHI 604D electrochemical workstation. The frequency was varied from 10^{-2} to 10^6 Hz with an amplitude of 5 mV.

2.4. Quantum Mechanical Calculations. The quantum mechanical calculations reported herein were performed on the basis of DFT within the generalized gradient approximation (GGA-PW91),[41] as implemented in the Vienna Ab Initio Simulation Package (VASP).[42−44] The projector augmented wave (PAW) method with a planewave basis set was employed to describe the interaction between ion cores and valence electrons. Valence configurations employed are $3s^1$ for Na and $4s^24p^2$ for Ge. An energy cutoff of 200 eV was applied for the planewave expansion of the electronic eigenfunctions. During geometry optimization, all atoms were fully relaxed using the conjugate gradient method until residual forces on constituent atoms become smaller than 5×10^{-2} eV/Å. For Brillouin zone sampling, a $(2 \times 2 \times 2)$ k-point mesh in the scheme of Monkhorst-Pack[45] was used for all bulk amorphous samples, and for the corresponding slab models, a $(2 \times 2 \times 1)$ k-point mesh was used.

3. RESULTS AND DISCUSSION

A scanning electron microscope (SEM) image of a germanium film deposited at 70° off-normal is shown in Figure 1. The film

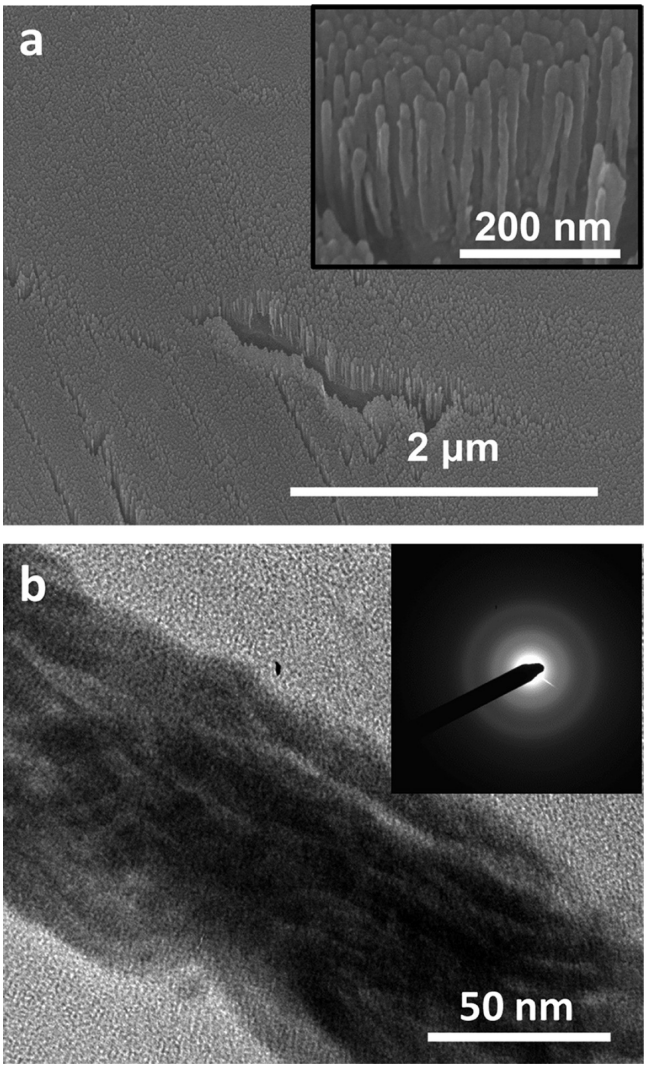

Figure 1. (a) SEM image of germanium nanocolumns deposited at 70°. (b) HRTEM image of a bundle of nanocolumns. The inset shows the electron diffraction pattern from the material.

exhibits nanocolumnar morphology with individual columns having a diameter of ~20 nm. The small diameter of the individual columns serves to buffer the volumetric expansion undergone during sodium insertion. Despite germanium's modest sodium capacity, the volumetric expansion associated with the formation of NaGe is greater than 100%.[46] Additionally, the small columnar diameter provides a short ion-diffusion length, which facilitates rapid sodium insertion and extraction. An HRTEM image of a bundle of individual columns is shown in Figure 1b. No lattice fringes are visible, indicating that the as-deposited material is amorphous. Amorphous nanocolumns are expected, as the growth of

dx.doi.org/10.1021/jp407322k | J. Phys. Chem. C 2013, 117, 18885−18890

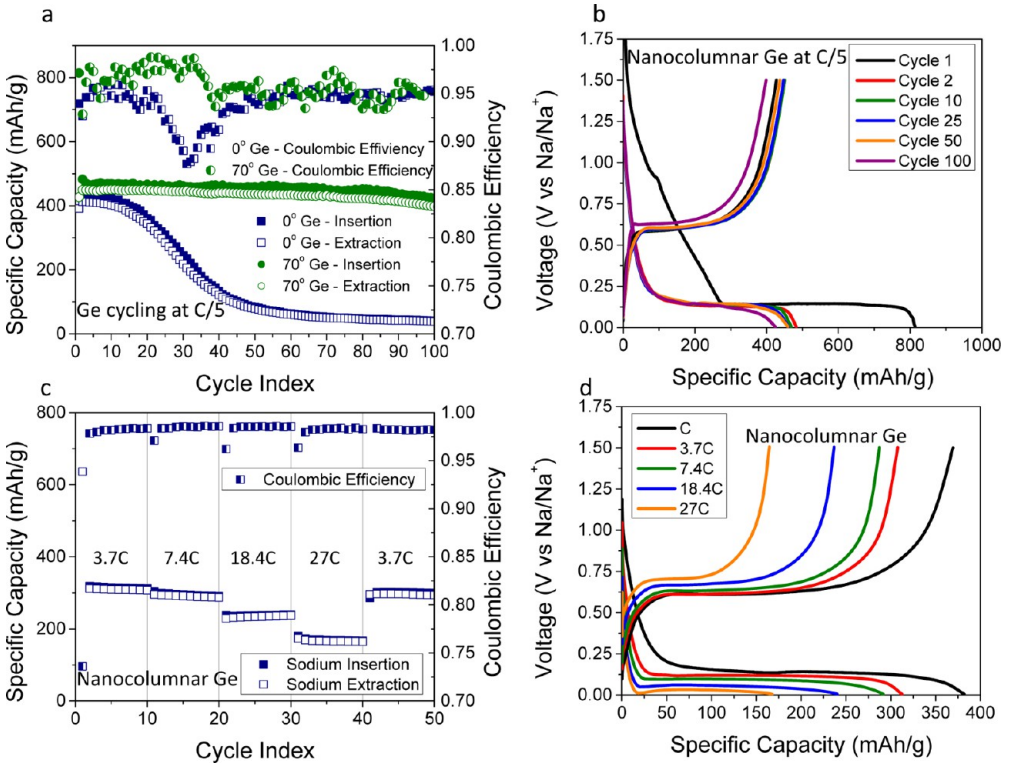

Figure 2. (a) Cycling results for germanium thin films deposited at an incident angle of 0 and 70°. Cycling was performed at C/5 after an initial conditioning cycle of C/20. (b) Voltage profiles for the 1st, 2nd, 10th, 25th, 50th, and 100th sodium insertion cycles in nanocolumnar germanium deposited at 70°. (c) C-rate testing of 70° germanium thin films with 10 cycles each at 3.7C, 7.4C, 18.4C, and 27C (10 A/g), and (d) voltage profiles for sodium insertion cycles at each rate in the C-rate test.

crystalline or poly crystalline material requires adatom surface diffusion in order to build long-range order into the structures. This requirement for crystalline growth contradicts the requirements required for the growth of nanocolumnar films by GLAD.[40] The amorphous nature of the material was confirmed by selected-area electron diffraction, shown in the insert in Figure 1b. Only diffuse rings are present indicating the lack of any long-range order in the sample. SEM images of the dense films deposited at 0° as well as a clean stainless steel substrate are shown in Figure S2. These films do not exhibit nanostructuring. Any features in the film are the result of substrate roughness being conformally coated during deposition.

Coin cells were made with both nanocolumnar and dense germanium film anodes charged/discharged versus sodium metal counterelectrodes. The cycle life testing results are shown in Figure 2a. The cycling was at C/5 after an initial conditioning cycle at C/20. While the initial capacities of the dense and nanocolumnar films are similar (430 mAh/g for the nanocolumnar films versus 400 mAh/g for the dense films), the stability of the two morphologies are markedly different. The nanocolumnar film, deposited at 70°, shows excellent capacity retention, maintaining 88% of initial capacity after 100 cycles. The dense film, however, begins to show significant capacity fade after only 15 cycles. SEM imaging of cycled dense electrodes revealed significant cracking after a single cycle with additional cracking and delamination occurring by the fifth cycle (see Figure S3). The dense films also have a lower average coulombic efficiency than the nanocolumnar films (93 vs 95%). This is additional evidence of the dense film's pulverization, which exposes new surfaces for SEI formation. Maranchi et al. investigated the behavior of the a-Si/copper current collector interface, and concluded that the cracking and subsequent delamination of the active material was due to the accumulated plastic deformation of the substrate after multiple cycles.[47] The same mechanism is likely responsible for the failure of the dense films in this study. The cycling stability of the nanocolumnar film, deposited at 70°, is therefore the result of the nanoscale dimensions effectively buffering the stresses resulting from the volumetric expansion undergone during cycling both in the bulk and at the active material/substrate interface.

The voltage profiles for the reversible sodiation of germanium films deposited at 70° are shown in Figure 2b. The first sodium insertion shows a distinct voltage plateau at 130 mV versus sodium. This voltage is lower than the nearly 400 mV calculated by Chevrier and Ceder.[24] While the magnitude of the 130 mV plateau is too large to be consistent with the formation of the NaGe phase, it is consistent with the reversible capacity of the system, as seen in subsequent cycles. The sodium stripping plateau is located at ~600 mV. A large irreversible reaction during the first cycle sodiation includes a shoulder in the voltage profile at ~900 mV which we attribute to the onset of the formation of a passivating SEI layer. The shape of the sodiation and desodiation voltage profiles are quite flat which indicates that the sodiation reaction procedes via a two-phase reaction mechanism: a reaction front separating the sodium-rich and sodium-poor phases propagates through the material as the reaction progresses.

There is very little change in the shape of the sodiation curves between the first cycle and the 50th cycle, indicating that the sodiation reaction is reversible and that nanocolumnar

dx.doi.org/10.1021/jp407322k | J. Phys. Chem. C 2013, 117, 18885−18890

germanium has good stability when cycled at a slow rate. Between the 50th and 100th cycle, the capacity is lowered and there is a slight increase in the desodiation potential. The sodiation reaction terminates at Na_xGe with $x \approx 1.17$, and the small feature size in the nanocolumnar films is able to effectively buffer the large volumetric expansion associated with sodiation.[46] The product of electrochemical sodiation is not an equilibrium phase, as there are no phases between NaGe and Na_3Ge reported on the phase diagram. It is likely, as is the case with electrochemical lithiation of silicon, that the sodiation of germanium reaches a metastable terminal phase not found on the equilibrium phase diagram.[48,49]

X-ray photoelectron spectroscopy (XPS) was used to investigate the final composition of the sodiated electrodes. A dense germanium electrode was sodiated to 5 mV versus Na/Na^+ at a rate of C/10 and held at that voltage until the current decayed below C/100. The composition of the material was found to be 54 at% sodium and 46 at% germanium. These atomic ratios correspond to a sodium insertion capacity of 433 mAh/g, which is in very good agreement with the electrochemically derived value. The XPS spectrum for sodiated germanium is shown in Figure S4. Details on the elemental analysis can also be found in the Supporting Information. X-ray diffraction indicated that the sodiated germanium remained amorphous, precluding structural characterization of the sodiated germanium.

The sodium insertion capacity is consistently higher than the extraction capacity indicating that even though the electrode is stable, the SEI layer is not. While the addition of fluorinated ethylene carbonate as an electrolyte cosolvent for lithium-ion batteries significantly improves the coulombic efficiency for silicon and germanium electrodes owing to its formation of a superior SEI layer,[26,27,50,51] the SEI layer formed from a sodium-salt electrolyte appears to be less stable.

Figure 2c shows the cycling behavior of nanocolumnar germanium anodes cycled at various C-rates. After an initial conditioning cycle at C/20, the rate was increased to 3.7C, 7.4C, 18.4C, and 27C for 10 cycles each. The electrode exhibited a capacity of 307 mAh/g at 3.7C, 287 at 7.4C, 236 mAh/g at 18.4C, and 164 mAh/g at 27C. 27C corresponds to a current density of 10 A/g. The high capacity retention at high charge rates indicates that sodium diffusion is rapid in amorphous germanium despite the large radius of the sodium ion. Additionally, the high current capability on sodium insertion provides a measure of safety by making it difficult to electrodeposit sodium on the electrode surface. A C-rate test performed on a dense film is shown in Figure S5. The voltage profile for the last cycle at each C-rate is shown in Figure 2d. At the two highest current densities, a nucleation overpotential becomes apparent at the beginning of sodiation as a result of the two-phase reaction mechanism for the sodiation of germanium.

The impedance spectra of fully sodiated and fully desodiated dense germanium films are shown in Figure 3. The 20 nm thick dense films were used so that the electrode would have a well-defined surface area and a well-known finite diffusion length. The impedance spectra were fit to a modified Randle's circuit employing a constant phase element to account for surface roughness and a finite Warburg element to account for the solid state diffusion. From this model, the diffusion coefficient for sodium in the dense germanium film was found to be $\sim 9 \times 10^{-14}$ cm^2 s^{-1}, and the diffusion coefficient for sodium in sodiated germanium was found to be 1.6×10^{-13} cm^2 s^{-1}. This

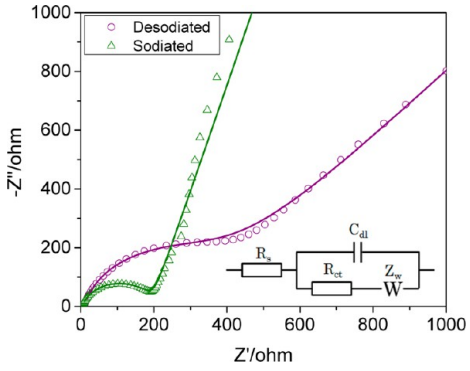

Figure 3. Impedance spectra of both fully sodiated (at 10 mV vs Na/Na^+) and fully desodiated (at 1 V vs Na/Na^+) 20 nm thick dense germanium films. The data were modeled using a Randles circuit. The data are shown as open symbols and the model fit is shown as solid lines.

is much faster than what is predicted by extrapolation from high temperature diffusion data for single-crystalline germanium.[30] The measured diffusion coefficient is not directly comparable to values for single-crystalline materials as the presence of surface and grain-boundary diffusion, as well as the amorphous nature of the material, have a significant impact on the apparent diffusion rate. Defects in amorphous semiconductors tend to trap interstitial diffusors such as sodium, thus slowing diffusion. However, the nanoscale thickness of the electrodes used for the impedance measurements results in a large surface area to volume ratio, thus, making surface diffusion a dominant effect.

To examine the surface effects on the mobility of Na atoms in sodiated Ge, ab initio molecular dynamics (AIMD) simulations were performed at 1000 K to calculate Na diffusivities (D_{Na}) in slab and bulk amorphous $Na_{0.25}Ge_{0.75}$ alloy (a-$Na_{0.25}Ge_{0.75}$) systems. The bulk model structure for a-$Na_{0.25}Ge_{0.75}$ consisting of 16 Na and 48 Ge atoms was created with AIMD simulations. Detailed computational methods can be found elsewhere.[52,53] The slab models had a 15-Å-thick vacuum gap inserted into the a-$Na_{0.25}Ge_{0.75}$ bulk alloys in the z direction. To simulate a laterally extended surface in the x and y directions, we employed the repeated-slab approach by applying periodic boundary conditions to the unit cell. The unit cells for the bulk and slab systems are illustrated in Figure 4.

For each system, three samples were averaged to calculate the mean-square displacements of Na atoms ($MSD = |R_i(t) - R_i(0)|^2$, where $R_i(t)$ is the position of atom i at time t). From the MSD profiles shown in Figure 5, D_{Na} values were obtained

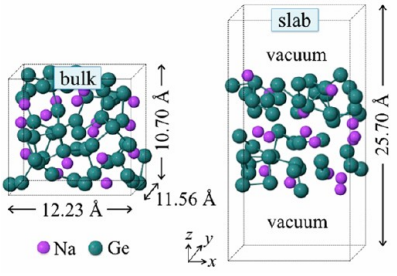

Figure 4. Side view of a-$Na_{0.25}Ge_{0.75}$ bulk and slab systems each containing 64 atoms. The laterally extended surface in the x and y directions is simulated using the repeated slab approach with a vacuum layer inserted in the z direction.

dx.doi.org/10.1021/jp407322k | J. Phys. Chem. C 2013, 117, 18885−18890

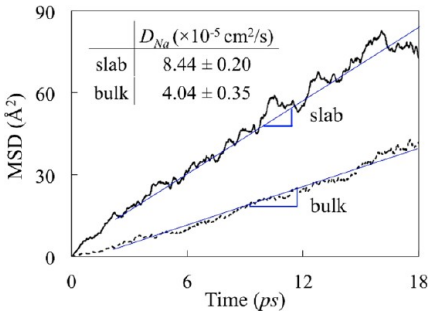

Figure 5. Variation in the mean square displacements (MSDs) of Na atoms in a-$Na_{0.25}Ge_{0.75}$ bulk and slab systems at 1000 K.

from the Einstein relation, $D = \langle MSD \rangle / 6t$; the angular bracket denotes an averaged value. Here, the MD duration of 18 ps appears to be sufficient to obtain well-converged results; disregarding the first 2 ps, linear fits over a time interval of the following 16 ps yield $D_{Na} = 8.44 \pm 0.20$ and $4.03 \pm 0.35 \times 10^{-5}$ cm^2/s for the slab and bulk systems, respectively. Although the slabs employed in our calculations were fairly thin, we could not exclude the contribution of the (bulk-like) subsurface/center regions; hence, the diffusivities calculated here should not be viewed as pure surface diffusivities. Nevertheless, the results clearly show that Na diffusion along the surface is much more facile than bulk diffusion. As a result, the nanocolumnar Ge thin films with a relatively large surface-area-to-volume ratio are able to sustain reversible charge/discharge rates as high as 27C (10 A/g).

4. CONCLUSIONS

We have demonstrated the reversible electrochemical storage of sodium in nanocolumnar germanium electrodes with an initial sodium storage capacity of 430 mAh/g. After 100 cycles at C/5, 88% of this capacity is retained. The material also exhibits high capacity retention at rates up to 27C (10 A/g). Dense germanium films exhibit significant capacity fade when cycled at the same rate. Ab initio molecular dynamics simulations of the Na−Ge system indicate that near-surface diffusion is significantly faster than bulk diffusion. Nanoscale dimensions, therefore, are critical for stable, reversible, and high-rate sodiation of germanium.

■ ASSOCIATED CONTENT

Supporting Information

Additional figures and text describing the deposition and electrochemical behavior and characterization of dense germanium films. This material is available free of charge via the Internet at http://pubs.acs.org.

■ AUTHOR INFORMATION

Corresponding Author

*Tel.: 512-471-5817. Fax: 512-471-7060. E-mail: mullins@che.utexas.edu.

Notes

The authors declare no competing financial interest.

■ ACKNOWLEDGMENTS

This work was supported by the Welch Foundation (Grant F-1436 for C.B.M., F-1131 for A.H., F-1535 for G.S.H., and F-1066 for J.B.G.). Additionally, P.R.A. thanks the Hertz foundation for a Graduate Fellowship, and Y.M.L. thanks the University of Texas at Austin for a Powers Graduate Fellowship. Finally, Solvay Special Chemicals is thanked for providing the FEC and Celgard for the separator material employed in these studies.

■ REFERENCES

(1) Wen, Z.; Hu, Y.; Wu, X.; Han, J.; Gu, Z. Main Challenges for High Performance NAS Battery: Materials and Interfaces. *Adv. Funct. Mater.* **2012**, *23*, 1005−1018.

(2) Lu, X.; Li, G.; Kim, J. Y.; Lemmon, J. P.; Sprenkle, V. L.; Yang, Z. The Effects of Temperature on the Electrochemical Performance of Sodium−Nickel Chloride Batteries. *J. Power Sources* **2012**, *215*, 288−295.

(3) Ellis, B. L.; Nazar, L. F. Sodium and Sodium-Ion Energy Storage Batteries. *Curr. Opin. Solid State Mater. Sci.* **2012**, *16*, 168−177.

(4) Moreau, P.; Guyomard, D.; Gaubicher, J.; Boucher, F. Structure and Stability of Sodium Intercalated Phases in Olivine $FePO_4$. *Acc. Chem. Res.* **2010**, *22*, 4126−4128.

(5) Liu, Y.; Xu, Y.; Han, X.; Pellegrinelli, C.; Zhu, Y.; Zhu, H.; Wan, J.; Chung, A. C.; Vaaland, O.; Wang, C.; et al. Porous Amorphous $FePO_4$ Nanoparticles Connected by Single-Wall Carbon Nanotubes for Sodium Ion Battery Cathodes. *Nano Lett.* **2012**, *12*, 5664−5668.

(6) Kim, D.; Lee, E.; Slater, M.; Lu, W.; Rood, S.; Johnson, C. S. Layered $Na[Ni_{1/3}Fe_{1/3}Mn_{1/3}]O_2$ Cathodes for Na-Ion Battery Application. *Electrochem. Commun.* **2012**, *18*, 66−69.

(7) Xia, X.; Dahn, J. R. $NaCrO_2$ is a Fundamentally Safe Positive Electrode Material for Sodium-Ion Batteries with Liquid Electrolytes. *Electrochem. Solid-State Lett.* **2012**, *15*, A1−A4.

(8) Barpanda, P.; Ye, T.; Nishimura, S.-I.; Chung, S.-C.; Yamada, Y.; Okubo, M.; Zhou, H.; Yamada, A. Sodium Iron Pyrophosphate: A Novel 3.0 V Iron-Based Cathode for Sodium-Ion Batteries. *Electrochem. Commun.* **2012**, *24*, 116−119.

(9) Sun, Q.; Ren, Q.-Q.; Fu, Z.-W. NASICON-Type $Fe_2(MoO_4)_3$ Thin Film as Cathode for Rechargeable Sodium Ion Battery. *Electrochem. Commun.* **2012**, *23*, 145−148.

(10) Jian, Z.; Zhao, L.; Pan, H.; Hu, Y.-S.; Li, H.; Chen, W.; Chen, L. Carbon Coated $Na_3V_2(PO_4)_3$ as Novel Electrode Material for Sodium Ion Batteries. *Electrochem. Commun.* **2012**, *14*, 86−89.

(11) Lim, S. Y.; Kim, H.; Shakoor, R. A.; Jung, Y.; Choi, J. W. Electrochemical and Thermal Properties of NASICON Structured $Na_3V_2(PO_4)_3$ as a Sodium Rechargeable Battery Cathode: A Combined Experimental and Theoretical Study. *J. Electrochem. Soc.* **2012**, *159*, A1393−A1397.

(12) Lu, Y.; Wang, L.; Cheng, J.; Goodenough, J. B. Prussian Blue: a New Framework of Electrode Materials for Sodium Batteries. *Chem. Commun.* **2012**, *48*, 6544−6546.

(13) Wessells, C. D.; Peddada, S. V.; Huggins, R. A.; Cui, Y. Nickel Hexacyanoferrate Nanoparticle Electrodes For Aqueous Sodium and Potassium Ion Batteries. *Nano Lett.* **2011**, *11*, 5421−5425.

(14) Wessells, C. D.; McDowell, M. T.; Peddada, S. V.; Pasta, M.; Huggins, R. A.; Cui, Y. Tunable Reaction Potentials in Open Framework Nanoparticle Battery Electrodes for Grid-Scale Energy Storage. *ACS Nano* **2012**, *6*, 1688−1694.

(15) Alcántara, R.; Jiménez-Mateos, J. M.; Lavela, P.; Tirado, J. L. Carbon Black: A Promising Electrode Material for Sodium-Ion Batteries. *Electrochem. Commun.* **2001**, *3*, 639−642.

(16) Wenzel, S.; Hara, T.; Janek, J.; Adelhelm, P. Room-Temperature Sodium-Ion Batteries: Improving the Rate Capability of Carbon Anode Materials by Templating Strategies. *Energy Environ. Sci.* **2011**, *4*, 3342−3345.

(17) Cao, Y.; Xiao, L.; Sushko, M. L.; Wang, W.; Schwenzer, B.; Xiao, J.; Nie, Z.; Saraf, L. V.; Yang, Z.; Liu, J. Sodium Ion Insertion in Hollow Carbon Nanowires for Battery Applications. *Nano Lett.* **2012**, *12*, 3783−3787.

(18) Ellis, L. D.; Hatchard, T. D.; Obrovac, M. N. Reversible Insertion of Sodium in Tin. *J. Electrochem. Soc.* **2012**, *159*, A1801−A1805.

(19) Datta, M. K.; Epur, R.; Saha, P.; Kadakia, K.; Park, S. K.; Kumta, P. N. Tin and Graphite Based Nanocomposites: Potential Anode for Sodium Ion Batteries. *J. Power Sources* **2013**, *225*, 316−322.
(20) Lin, Y.-M.; Abel, P. R.; Gupta, A.; Goodenough, J. B.; Heller, A.; C. B. Mullins Sn-Cu Alloy Anodes for Rechargeable Sodium Ion Batteries. *ACS Appl. Mater. Interfaces* **2013**, accepted for publication.
(21) Qian, J.; Chen, Y.; Wu, L.; Cao, Y.; Ai, X.; Yang, H. High Capacity Na-Storage and Superior Cyclability of Nanocomposite Sb/C Anode for Na-Ion Batteries. *Chem. Commun.* **2012**, *48*, 7070−7072.
(22) Darwiche, A.; Marino, C.; Sougrati, M. T.; Fraisse, B.; Stievano, L.; Monconduit, L. Better Cycling Performances of Bulk Sb in Na-Ion Batteries Compared to Li-Ion Systems: An Unexpected Electrochemical Mechanism. *J. Am. Chem. Soc.* **2012**, *134*, 20805−20811.
(23) Xiao, L.; Cao, Y.; Xiao, J.; Wang, W.; Kovarik, L.; Nie, Z.; Liu, J. High Capacity, Reversible Alloying Reactions in SnSb/C Nanocomposites for Na-Ion Battery Applications. *Chem. Commun.* **2012**, *48*, 3321−3323.
(24) Chevrier, V. L.; Ceder, G. Challenges for Na-Ion Negative Electrodes. *J. Electrochem. Soc.* **2011**, *158*, A1011−A1014.
(25) Abel, P. R.; Chockla, A. M.; Lin, Y.-M.; Holmberg, V. C.; Harris, J. T.; Korgel, B. A.; Heller, A.; Mullins, C. B. Nanostructured $Si_{(1-x)}Ge_x$ for Tunable Thin Film Lithium-Ion Battery Anodes. *ACS Nano* **2013**, *7*, 2249−2257.
(26) Chockla, A. M.; Klavetter, K. C.; Mullins, C. B.; Korgel, B. A. Solution-Grown Germanium Nanowire Anodes for Lithium-Ion Batteries. *ACS Appl. Mater. Interfaces* **2012**, *4*, 4658−4664.
(27) Klavetter, K. C.; Wood, S. M.; Lin, Y.-M.; Snider, J. L.; Davy, N. C.; Chockla, A. M.; Romanovicz, D. K.; Korgel, B. A.; Lee, J.-W.; Heller, A.; et al. A High-Rate Germanium-Particle Slurry Cast Li-Ion Anode with High Coulombic Efficiency and Long Cycle Life. *J. Power Sources* **2013**, *238*, 123−136.
(28) Graetz, J.; Ahn, C. C.; Yazami, R.; Fultz, B. Nanocrystalline and Thin Film Germanium Electrodes with High Lithium Capacity and High Rate Capabilities. *J. Electrochem. Soc.* **2004**, *151*, A698−A702.
(29) Chan, C. K.; Zhang, X. F.; Cui, Y. High Capacity Li Ion Battery Anodes Using Ge Nanowires. *Nano Lett.* **2007**, *8*, 307−309.
(30) Stojić, M.; Kostić, D.; Stošić, B. The Behaviour of Sodium in Ge, Si and GaAs. *Physica B* **1986**, *138*, 125−128.
(31) Fuller, C. S.; Severiens, J. C. Mobility of Impurity Ions in Germanium and Silicon. *Phys. Rev.* **1954**, *96*, 21−24.
(32) Abelmann, L.; Lodder, C. Oblique Evaporation and Surface Diffusion. *Thin Solid Films* **1997**, *305*, 1−21.
(33) Robbie, K.; Sit, J. C.; Brett, M. J. Advanced Techniques for Glancing Angle Deposition. *J. Vac. Sci. Technol., B* **1998**, *16*, 1115−1122.
(34) Flaherty, D. W.; Dohnálek, Z.; Dohnálková, A.; Arey, B. W.; McCready, D. E.; Ponnusamy, N.; Mullins, C. B.; Kay, B. D. Reactive Ballistic Deposition of Porous TiO_2 Films: Growth and Characterization. *J. Phys. Chem. C* **2007**, *111*, 4765−4773.
(35) Krause, K. M.; Thommes, M.; Brett, M. J. Pore Analysis of Obliquely Deposited Nanostructures by Krypton Gas Adsorption at 87 K. *Microporous Mesoporous Mater.* **2011**, *143*, 166−173.
(36) Fleischauer, M. D.; Li, J.; Brett, M. J. Columnar Thin Films for Three-Dimensional Microbatteries. *J. Electrochem. Soc.* **2009**, *156*, A33−A36.
(37) Abel, P. R.; Lin, Y.-M.; Celio, H.; Heller, A.; Mullins, C. B. Improving the Stability of Nanostructured Silicon Thin Film Lithium-Ion Battery Anodes through Their Controlled Oxidation. *ACS Nano* **2012**, *6*, 2506−2516.
(38) Lin, Y.-M.; Abel, P. R.; Flaherty, D. W.; Wu, J.; Stevenson, K. J.; Heller, A.; Mullins, C. B. Morphology Dependence of the Lithium Storage Capability and Rate Performance of Amorphous TiO_2 Electrodes. *J. Phys. Chem. C* **2011**, *115*, 2585−2591.
(39) Flaherty, D. W.; Hahn, N. T.; May, R. A.; Berglund, S. P.; Lin, Y.-M.; Stevenson, K. J.; Dohnalek, Z.; Kay, B. D.; Mullins, C. B. Reactive Ballistic Deposition of Nanostructured Model Materials for Electrochemical Energy Conversion and Storage. *Acc. Chem. Res.* **2012**, *45*, 434−443.
(40) Hawkeye, M. M.; Brett, M. J. Glancing Angle Deposition: Fabrication, Properties, and Applications of Micro- and Nanostructured Thin Films. *J. Vac. Sci. Technol., A* **2007**, *25*, 1317−1335.
(41) Blöchl, P. E. Projector Augmented-Wave Method. *Phys. Rev. B* **1994**, *50*, 17953−17979.
(42) Kresse, G.; Hafner, J. Ab Initio Molecular Dynamics for Liquid Metals. *Phys. Rev. B* **1993**, *47*, 558−561.
(43) Kresse, G.; Furthmüller, J. Efficiency of Ab Initio Total Energy Calculations for Metals and Semiconductors Using a Plane-Wave Basis Set. *Comput. Mater. Sci.* **1996**, *6*, 15−50.
(44) Kresse, G.; Furthmüller, J. Efficient Iterative Schemes for Ab Initio Total-Energy Calculations Using a Plane-Wave Basis Set. *Phys. Rev. B* **1996**, *54*, 11169−11186.
(45) Monkhorst, H. J.; Pack, J. D. Special Points for Brillouin-Zone Integrations. *Phys. Rev. B* **1976**, *13*, 5188−5192.
(46) Witte, J.; Schnering, H. G.; Klemm, W. Das Verhalten der Alkalimetalle zu Halbmetallen. XI. Die Kristallstruktur von NaSi und NaGe. *Z. Anorg. Allg. Chem.* **1964**, *327*, 260−273.
(47) Maranchi, J. P.; Hepp, A. F.; Evans, A. G.; Nuhfer, N. T.; Kumta, P. N. Interfacial Properties of the *a*-Si/Cu:Active−Inactive Thin-Film Anode System for Lithium-Ion Batteries. *J. Electrochem. Soc.* **2006**, *153*, A1246−A1253.
(48) Hatchard, T. D.; Dahn, J. R. In Situ XRD and Electrochemical Study of the Reaction of Lithium with Amorphous Silicon. *J. Electrochem. Soc.* **2004**, *151*, A838−A842.
(49) Obrovac, M. N.; Christensen, L. Structural Changes in Silicon Anodes during Lithium Insertion/Extraction. *Electrochem. Solid-State Lett.* **2004**, *7*, A93−A96.
(50) Lin, Y.-M.; Klavetter, K. C.; Abel, P. R.; Davy, N. C.; Snider, J. L.; Heller, A.; Mullins, C. B. High Performance Silicon Nanoparticle Anode in Fluoroethylene Carbonate-Based Electrolyte for Li-Ion Batteries. *Chem. Commun.* **2012**, *48*, 7268−7270.
(51) Nakai, H.; Kubota, T.; Kita, A.; Kawashima, A. Investigation of the Solid Electrolyte Interphase Formed by Fluoroethylene Carbonate on Si Electrodes. *J. Electrochem. Soc.* **2011**, *158*, A798−A801.
(52) Chou, C.-Y.; Hwang, G. S. Surface Effects on the Structure and Lithium Behavior in Lithiated Silicon: A First Principles Study. *Surf. Sci.* **2013**, *612*, 16−23.
(53) Kim, H.; Chou, C.-Y.; Ekerdt, J. G.; Hwang, G. S. Structure and Properties of Li−Si Alloys: A First-Principles Study. *J. Phys. Chem. C* **2011**, *115*, 2514−2521.